

Postprocessing seasonal weather forecasts

Claudio Heinrich, Kristoffer H. Hellton, Alex Lenkoski and

Thordis L. Thorarinsdottir*

Norwegian Computing Center, Oslo, Norway

March 10, 2022

Abstract

Seasonal weather forecasts are crucial for long-term planning in many practical situations and skillful forecasts may have substantial economic and humanitarian implications. Current seasonal forecasting models require statistical postprocessing of the output to correct systematic biases and unrealistic uncertainty assessments. We propose a multivariate postprocessing approach utilizing covariance tapering, combined with a dimension reduction step based on principal component analysis for efficient computation. Our proposed technique can correctly and efficiently handle non-stationary, non-isotropic and negatively correlated spatial error patterns, and is applicable on a global scale. Further, a moving average approach to marginal postprocessing is shown to flexibly handle trends in biases caused by global warming,

*The authors gratefully acknowledge the support of the Volkswagen Foundation through grant nr. 88511 and the Research Council of Norway through grant nr. 270733. We thank Tilmann Gneiting and our project partners in the Seasonal Forecasting Engine project for fruitful discussions.

and short training periods. In an application to global sea surface temperature forecasts issued by the Norwegian Climate Prediction Model (NorCPM), our proposed methodology is shown to outperform known reference methods.

Keywords: Covariance regularization, moving average, multivariate postprocessing, probabilistic forecast, sea surface temperature

1 Introduction

Seasonal, or medium-range, weather forecasts on a timescale of one month to a year ahead are highly important in a range of applications. Decision makers can e.g. greatly benefit from skillful forecasts of increased danger for natural disasters or extreme weather events, such as droughts, hurricanes or extreme snowfall and winds, for efficient mitigation efforts and emergency management. Unlike short-range weather forecasting, medium-range forecasts rely on the prediction of atmospheric modes with a low-frequency variability which can be predicted months ahead. This includes the El Niño Southern Oscillation, monsoon rains and the Northern Atlantic Oscillation (Hoskins, 2013). As ocean states change considerably slower than states in the atmosphere, these modes are typically associated with the sea surface temperature in certain regions. Therefore, reliable months-ahead forecasting of sea surface temperature is a crucial first step towards skillful seasonal forecasts of other weather phenomena. For example, the winter mean surface temperature in large parts of Europe is considered to be negatively correlated with the sea surface temperature in the Nordic seas in the preceding autumn (Kolstad and Årthun, 2018; Dobrynin et al., 2018).

In order to be useful for decision-making, weather forecasts ought to be probabilistic in nature and well calibrated (Gneiting et al., 2007). Calibration implies that the probability of any event under the forecast distribution matches the actual frequency observed for the event. Current numerical weather prediction (NWP) models are typically deterministic and account for forecast uncertainty by generating an ensemble of forecasts where every

ensemble member represents a possible simulation of the future, often generated by creating a small perturbation of the initial state of the prediction. However, as these models rely on simplifications of the underlying physical system, a (possibly too crude) discretization of space and imperfect initialization, they will be biased. Further, the ensemble spread may not accurately capture the forecast uncertainty. Hence statistical postprocessing is required, where the forecast model is recalibrated based on past performance and observations, see Vannitsem et al. (2018) for an overview.

In the postprocessing of medium-range forecasts, obtaining enough training data is a particular challenge. The high-frequency variability patterns needs to be filtered out, such that observations have to be averaged over several weeks or months. As the period of reliable sea surface temperature observations starts around 1980, the beginning of the satellite era, the number of available observations for each season is typically below 50. Therefore, medium-range postprocessing techniques must be robust to minimize the risk of overfitting. Additionally, the ongoing climate change leads to significant trends in biases and model uncertainty over time (Van Schaeybroeck and Vannitsem, 2018).

Many questions stated by forecast users share the feature that they depend on the forecast distribution at *multiple* locations, so that the forecast must take into account complex dependencies for a skillful prediction of the answers. Examples include predicting the probability of the maximal sea surface temperature in a specific area exceeding 26.5°C , a necessary condition for the development of tropical cyclones (McTaggart-Cowan et al., 2015), or predicting the probability of observing sea ice along a shipping route. This requires multivariate postprocessing techniques.

A common approach to multivariate postprocessing is to fit variograms of a parametric covariance family, such as exponential covariance functions (e.g. Feldmann et al., 2015). This approach generally assumes stationarity and often nonnegative correlations decaying with distance. Neither of these assumptions are natural when considering global sea surface temperature, as it is likely to depend on ocean currents and the presence or absence of land

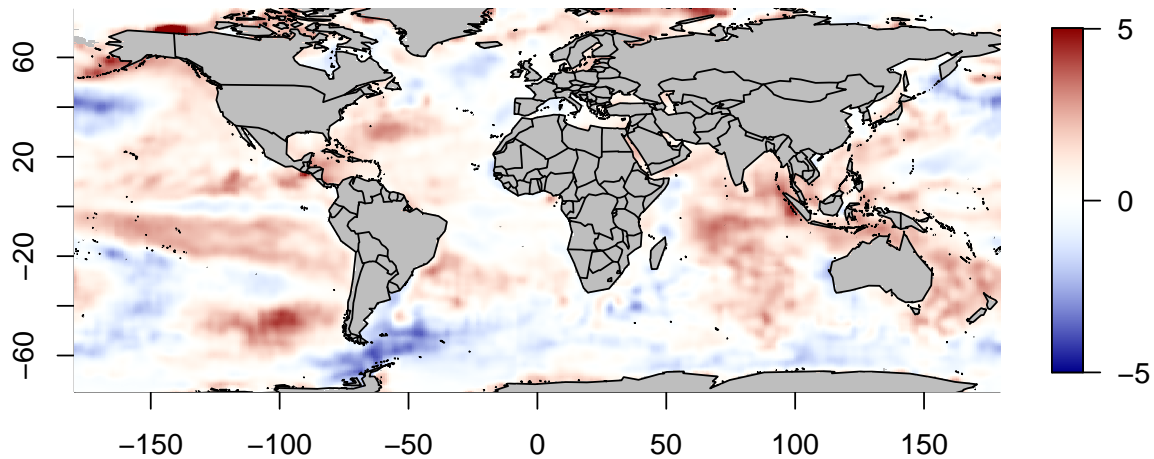


Figure 1: Normalized observed sea surface temperature for May 2016 where the normalisation is based on all available observations for May prior to 2016.

near, or in between, locations. This is highlighted by Figure 1 showing normalized observed sea surface temperature for May 2016. Nonstationary effects are visible, such as the strong horizontal correlations in the Pacific ocean westwards of Peru and Columbia due to the El Nino Southern Oscillation. These effects commonly carry forward to the forecast errors in that the model captures the pattern but not the exact magnitude.

Given the physical complexity underlying the NWP model, forecast residuals of different locations may be negatively correlated. For example, the sea surface temperature forecast in our data set for July tends to underestimate the temperature in the Baltic sea, when overestimating the temperature in the Barents sea, and vice versa. Most parametric families are not able to model negative correlations, an exception being parametric hole effect models (e.g. Chilès and Delfiner, 1999). However, these assume that locations at certain distances are always negatively correlated, which is not reasonable in our setup.

We propose a probabilistic multivariate postprocessing approach to tackle these issues

and apply it to forecasts of monthly mean sea surface temperature issued by the Norwegian climate prediction model (NorCPM). A moving average approach ensures that the postprocessing will be robust against lack of training data and trends in biases and uncertainties caused by climate change. To achieve spatially consistent forecasts, we explicitly model the spatial dependence structure of the forecast residuals. We utilize regularization of the covariance structure by tapering the covariance matrix, and use further dimension reduction based on principal component analysis to reduce the computational time and reduce the risk of overfitting. Validation on out-of-sample observational data demonstrates that this multivariate postprocessing approach yields spatially consistent and well calibrated forecasts.

The paper is organized as follows: in Section 2, we first develop a univariate postprocessing technique based on moving averages, and extend this to the multivariate setting, incorporating covariance tapering, principal component analysis and a marginal variance correction. Section 3 outlines several validation and comparison tools for multivariate forecast distributions. In Section 4, we show how the proposed univariate and multivariate methods perform for the NorCPM forecasts and compare their performance to several reference methods. In Section 5, we consider a case study of a shipping route in the Northern Atlantic, forecasting the probability of ice along the route. The Section 6 gives the concluding remarks and discussion of results. The code for all our methods is available as R package at www.github.com/ClaudioHeinrich/PostprocessingSST.

2 Modeling sea surface temperature

2.1 Data

We consider monthly mean forecasts of sea surface temperature (SST) issued by the Norwegian climate prediction model (NorCPM), see Counillon et al. (2014, 2016). The forecasts

cover the entire globe on a longitude-latitude grid with resolution 1° , for a total of 64 800 grid points, where approximately 43 000 are located in the oceans. NorCPM issues new forecasts every 3 months, at the beginning of January, April, July and October, such that the lead times of the forecasts vary between one and three months. Each forecast consists of nine exchangeable members. For postprocessing, we consider forecasts from 1985 to 2016. The validation period is set to 2001–2016, while the years 1985–2000 are used to train the model. Throughout the validation period, the model estimation is updated for each time point to include the most recent observations. Observations of monthly mean SST over the period are obtained from the Optimum Interpolation Sea Surface Temperature (OISST) dataset of the National Oceanic and Atmospheric Administration (Reynolds et al., 2007).

2.2 Univariate postprocessing

A wide range of methods are available for univariate forecast postprocessing, e.g. ensemble Bayesian model averaging, nonhomogeneous regressions and quantile regression; see Wilks (2018) for a recent overview. In our data set, both bias and prediction uncertainty depend strongly on spatial location and calendar month. Here, we postprocess data from each calendar month separately, ignoring possible interactions between months. In the following, a fixed month is considered with the monthly index suppressed for simplicity.

For a given year $y \in \{1985, \dots, 2016\}$ and location $s \in \mathcal{S}$, the SST *forecast* is assumed normally distributed,

$$X_{y,s} \sim \mathcal{N}(\mu_{y,s}, \sigma_{y,s}^2). \quad (1)$$

The mean and variance are estimated following a (weighted) moving average approach. Specifically, the mean is taken to be the bias-corrected NorCPM ensemble mean, $\hat{\mu}_{y,s} = \bar{f}_{y,s} - \hat{b}_{y,s}$, where \bar{f} denotes the mean of the raw ensemble. To account for trends in the bias over time, for instance caused by climatic changes not accounted for by NorCPM

and improved reliability of observations, the bias and predictive variance are estimated by weighted moving averages:

$$\hat{b}_{y,s} := \sum_{j < y} w_{y-j}^b (\bar{f}_{j,s} - t_{j,s}), \quad \hat{\sigma}_{y,s}^2 := \sum_{j < y} w_{y-j}^\sigma (t_{j,s} - (\bar{f}_{j,s} - \hat{b}_{j,s}))^2, \quad (2)$$

where $t_{j,s}$ denotes the *observed* temperature at year j and location s , and the sequences of weights $w_1, w_2 \dots$ are normalized. In Section 3, we compare the performance of a simple and an exponentially decaying weighting scheme. The weights for the bias are chosen by minimizing the mean squared error (MSE) of the bias-corrected forecast $\bar{f} - \hat{b}$. For the variance, they are chosen by minimizing the continuous rank probability score (CRPS). Note that this estimator does not rely on the spread of the forecast ensemble which is commonly used as predictor in short range weather forecasting (e.g. Messner et al., 2017). In seasonal to decadal forecasts the ensemble spread is known to be a less reliable predictor of forecast uncertainty (Ho et al., 2013). This is supported by the findings in Section 3.

In the OISST dataset, the SST is truncated at -1.79°C , the assumed freezing temperature of sea water. As this is relevant for relatively few grid points, we apply the same truncation to the predictive distributions after the parameter estimation rather than assuming a truncated normal model in (1). In numerical experiments, the truncation error was found to be substantially smaller than the forecast uncertainty. NorCPM, as most climate prediction models, will inherently account for global warming. However, it relies on simplification of the underlying physical processes and is unlikely to fully describe the effects of climate change. Moreover, numerical prediction models, once initialized, tend to drift towards a model attractor which on the seasonal to decadal scale introduces changes in model biases over time. While this may be accounted for with a linear trend term in the bias model (Boer, 2009), this was found to reduce the predictive ability here due to overfitting.

The proposed approach is compared against the related and well known non-homogeneous Gaussian regression (NGR) approach (Gneiting et al., 2005). Here, the mean and the vari-

ance are modeled as linear functions of predictor variables, most commonly the ensemble mean and the ensemble spread, i.e.

$$\widehat{\mu}_{y,s} = a + b\bar{f}_{y,s}, \quad \widehat{\sigma}_{y,s}^2 = c^2 + d^2 S_{y,s}^2,$$

where S^2 denotes the sample variance of the forecast ensemble, and a, b, c, d are regression coefficients. The coefficients a and b are fitted by linear regression by minimizing the mean squared error of the forecast, whereas c and d are fitted by minimizing the CRPS over the training period. In order to assess sensitivity to month and location, we consider three different versions of NGR for comparison: Grouped by month and location, $NGR_{m,s}$, where the coefficients may depend on both; grouped by location, NGR_s ; and grouped by month, NGR_m .

2.3 Multivariate postprocessing

In order to obtain physically consistent postprocessed forecast fields, the model (1) must be extended to include spatial correlation. The main challenge is that the set \mathcal{S} of considered locations contains around 42 000 points for the entire globe, and is very large compared to the sample size of up to 31 training years. To allow for non-stationary effects and negative correlations, we propose a postprocessing procedure based on regularization of the sample covariance matrix. It relies on a combination of tapering the sample covariance matrix and principal component analysis (PCA). These are classical tools for high-dimensional covariance estimation, but have found little attention in the context of statistical post-processing of spatial data. As reference methods we compare the proposed technique to a geostationary approach (Feldmann et al., 2015) and ensemble copula coupling (Scheffzik et al., 2013).

2.3.1 Post-processing by regularization of the sample covariance matrix

The univariate model (1) is extended by estimating the covariance matrix of the forecast residuals. The residuals are assumed to follow a multivariate normal distribution

$$\text{res}_y := t_y - \hat{\mu}_y \sim \mathcal{N}_S(0, \Sigma_y), \quad \text{with} \quad \text{diag}(\Sigma_y) = (\hat{\sigma}_{y,s_i}^2)_{s_i \in \mathcal{S}}, \quad (3)$$

where $\hat{\mu}_y$ denotes the vector of bias-corrected forecasts $\bar{f}_y - \hat{b}_y$, and t_y the vector of observed temperatures. The covariance matrix Σ_y is multi-layered as it captures both the spatial climatological correlation between different locations on the globe and the forecast uncertainty including spatial interactions. Given an estimator of the covariance matrix, $\hat{\Sigma}_y$, a spatial forecast is issued as

$$X_y \sim \mathcal{N}_S(\hat{\mu}_y, \hat{\Sigma}_y), \quad (4)$$

generalizing the marginal model in Equation (1). In the following, the year and month are assumed fixed and the indices y and m are suppressed.

The standard estimator of the covariance matrix is the sample covariance matrix (SCM):

$$\mathbf{S}(s_i, s_j) := \frac{1}{Y-1} \sum_y (t_{y,s_i} - \hat{\mu}_{y,s_i})(t_{y,s_j} - \hat{\mu}_{y,s_j}),$$

where the sum runs over all Y previously observed years. However, in the high-dimensional setting with limited training data, the sample covariance estimator requires regularization. We propose a two-step procedure for regularizing \mathbf{S} , first applying a distance-dependent tapering, or weighting, of the covariance matrix and secondly utilizing principal component analysis (PCA) to regularize the eigenstructure and reduce dimensionality.

For the first step, the tapering, we consider a positive, monotonically decreasing function ϕ , defining a spatial correlation function $C_\phi(s_i, s_j) = \phi(\|s_i - s_j\|)$ that only depends on the distance of the locations $s_i, s_j \in \mathcal{S}$. The SCM \mathbf{S} , is then tapered by ϕ by

$$\mathbf{S}_\phi(s_i, s_j) := \phi(\|s_i - s_j\|)\mathbf{S}(s_i, s_j).$$

The resulting tapered matrix is always positive semi-definite. Tapering covariance matrices by distances is frequently used in atmospheric sciences (Gaspari and Cohn, 1999). Gneiting (2002) argued that the weight function ϕ should be twice differentiable with $\phi'(0) = 0$ and a minimal second derivative $|\phi''(0)|$, and suggests the function

$$\phi_L(t) := \phi(t/L), \quad \text{where} \quad \phi(t) := \left((1-t) \frac{\sin(2\pi t)}{2\pi t} + \frac{1 - \cos(2\pi t)}{2\pi^2 t} \right) \mathbf{1}_{\{0 \leq t \leq 1\}}.$$

Here, ϕ is supported on $[0, 1]$, such that the tapering function ϕ_L has a tuning parameter L determining its support. In numerical experiments, the performance of our postprocessing method performed best for L between 1000km and 4000km. For the remaining of the paper, L is set to 2500km.

The tapering is beneficial in two ways: Firstly, the SCM does not consider distance between locations, and it will thus have a high risk of spurious correlations given the large number of locations pairs ($\sim 10^9$). The spatial correlation is likely to decrease with distance, and the tapering down-weights high correlations between distant locations as these are less credible than those between close locations. Secondly, it removes the rank deficiency of the SCM \mathbf{S} and changes it into a full rank matrix. Indeed, the rank of \mathbf{S} is limited by the number of observed years, $Y = 31$, significantly lower than $S = 42\,000$. The tapered covariance matrix having full rank makes it benefit more from regularization by principal component analysis (PCA).

To further reduce the risk of over-fitting and increase the speed of simulation, PCA is applied to the tapered covariance matrix estimate. PCA can be used to restrict the covariance estimator to a low-dimensional linear subspace with minimal information loss. In detail, we consider the eigenvalue decomposition of \mathbf{S}_ϕ

$$\mathbf{S}_\phi = U\Lambda U^T = \sum_{i=1}^S \lambda_i \mathbf{u}_i \mathbf{u}_i^T,$$

with orthogonal eigenvectors $U = [\mathbf{u}_1, \dots, \mathbf{u}_S]$ and eigenvalues $\Lambda = \text{diag}(\lambda_1, \dots, \lambda_S)$ in decreasing order.

The ordered eigenvectors, usually referred to as principal components, are orthogonal linear combinations of the locations expressing the highest variance. The underlying assumption is that only the first $d \ll S$ principal components truly represent a signal, whereas the variability of the remaining components represents unstructured noise. Therefore, only the first d eigenvectors are considered for the covariance estimate:

$$\tilde{\Sigma} := \sum_{i=1}^d \lambda_i \mathbf{u}_i \mathbf{u}_i^T.$$

The truncation of the eigenvalue decomposition will decrease the marginal sample variance at location s , the diagonal element \mathbf{S}_{ss} , for a given month:

$$\tilde{\Sigma}_{ss} = \sum_{i=1}^d \lambda_i \mathbf{u}_{is}^2 < \sum_{i=1}^S \lambda_i \mathbf{u}_{is}^2 = (\mathbf{S}_\phi)_{ss} = \mathbf{S}_{ss}. \quad (5)$$

Assuming the marginal postprocessing yields calibrated marginal distributions, we want the marginal variances of the multivariate method to equal those estimated by the univariate method. We will therefore compare two alternative approaches for correcting the variance deflation, a multiplicative and an additive correction. In the multiplicative correction, the PCA step is performed on the (tapered) correlation matrix and transformed back to the covariance matrix

$$\hat{\Sigma}^{mc} := \Xi \tilde{\Sigma} \Xi, \quad \text{with} \quad \Xi = \text{diag} \left(\frac{\hat{\sigma}_{y,1}}{(\tilde{\Sigma}_{11})^{1/2}}, \dots, \frac{\hat{\sigma}_{y,S}}{(\tilde{\Sigma}_{SS})^{1/2}} \right),$$

where the marginal variances $\hat{\sigma}_{y,s}^2$ are estimated as in (2).

Alternatively, we perform the PCA on the (tapered) covariance matrix and apply an additive correction to the marginal variances,

$$\hat{\Sigma}^{ac} := \tilde{\Sigma} + \text{diag}(\eta_1, \dots, \eta_S), \quad \text{where} \quad \eta_s := \max\{\hat{\sigma}_{y,s}^2 - \tilde{\Sigma}_{ss}, 0\}.$$

To ensure the positive definiteness of $\hat{\Sigma}^{ac}$, the difference between the regularized and unregularized marginal variances has to be truncated at zero. The additive correction does not

change the off-diagonal elements of $\tilde{\Sigma}$. It, however, only satisfies $\hat{\Sigma}_{ss}^{ac} = \hat{\sigma}_{y,s}^2$ for locations s where $\hat{\sigma}_{y,s}^2 \geq \tilde{\Sigma}_{ss}$. As the marginal estimator $\hat{\sigma}_{y,s}^2$ is not equal to the standard sample variance $(\mathbf{S})_{ss}$, this is not guaranteed for all locations.

The main purpose of applying PCA in this way is to prevent overfitting. In addition, the reduction of the rank allows for more efficient sampling from the predictive distribution. For instance, when simulating an S -dimensional normally distributed X with zero mean and covariance matrix $\hat{\Sigma}^{mc}$, it is sufficient to simulate a d -dimensional vector Y and set

$$X = \Xi U^{(d)} (\Lambda^{(d)})^{1/2} Y,$$

where $U^{(d)}$ and $\Lambda^{(d)}$ contain the first d eigenvectors and eigenvalues. We found that a dimension reduction with order of magnitude $S/d \approx 100$ leads to good results. As a consequence, simulating X with (previously computed) covariance matrix $\hat{\Sigma}^{mc}$ is approximately 100 times faster than simulating from a full rank normal distribution with known Cholesky-decomposition of the covariance matrix, disregarding fixed computation costs. This advantage is partly lost for the additive correction, as X is simulated by

$$X = U^{(d)} (\Lambda^{(d)})^{1/2} Y + \text{diag}(\eta_1, \dots, \eta_S) Z,$$

where Y is d -dimensional standard normal and Z is S -dimensional standard normal. This is nevertheless significantly faster than simulating from a general S -dimensional normal distribution.

2.3.2 Reference methods

We consider two reference methods commonly used in statistical postprocessing of spatial forecasts, see Schefzik and Möller (2018). A geostationary approach fits a parametric correlation model, assuming spatial stationarity and isotropy. The parametric correlation function is usually assumed to be in the Whittle-Matérn or the exponential family. Feldmann et al. (2015) suggest an exponential model with nugget, where the correlation of the

forecast error at locations s_i and s_j can be written as

$$C_{\theta,r}(s_i, s_j) = (1 - \theta) \exp\left(-\frac{\|s_i - s_j\|}{r}\right) + \theta \delta_{ij}.$$

The parameters θ and r are estimated by fitting the variogram of the parametric model to the empirical variogram, for details see Feldmann et al. (2015).

Secondly, we compare to ensemble copula coupling (ECC). The method constructs a postprocessed ensemble of the same size N as the original NWP ensemble. The new ensemble is univariately calibrated and follows the same rank-order structure as the raw NWP ensemble. This is achieved in two steps: First, a univariately calibrated ensemble $\tilde{x}^{(1)}, \dots, \tilde{x}^{(N)}$ is generated by considering m equally spaced quantiles of the calibrated distribution (1), i.e.

$$\tilde{x}_s^{(i)} := F_s^{-1}\left(\frac{i}{N+1}\right), \quad \text{for } i = 1, \dots, N, s = 1, \dots, S,$$

where F_s denotes the cumulative distribution function of the univariate model (1) at location s . Thereafter, the ensemble indices are permuted at each location to obtain an ensemble with the same rank order structure, or empirical copula, as the raw ensemble forecast. To achieve this, denote by $f_s^{(i)}$ the value of the i th ensemble member at location s of the raw forecast and find for each location a permutation ρ_s such that

$$f_s^{(\rho_s(1))} \leq \dots \leq f_s^{(\rho_s(N))}$$

is satisfied. Then, the i th member of the multivariate ECC forecast ensemble is

$$\{\tilde{x}_s^{(\rho_s^{-1}(i))}\}_{s \in \{1, \dots, S\}}.$$

For more details about ECC we refer to Schefzik et al. (2013). ECC is computationally efficient and it does not require the specification of a full multivariate distribution. A limitation is that the newly generated ensemble has the same number of members as the

NWP ensemble. While extensions to larger ensembles using the rank order structure of historical observations have been proposed (e.g. Schefzik, 2016), those do not apply in our setting of limited available historical observations.

3 Validation methods

We validate predictive performance by assessing the sharpness of the predictive distributions subject to calibration (Gneiting et al., 2007). Calibration, or reliability, refers to the statistical consistency between the forecast and the observations in the validation period, while sharpness refers to the spread of the predictive distribution. Subject to being calibrated, a sharper forecast is less uncertain and thus more informative.

Following Dawid (1984), probabilistic calibration of marginal forecasts is assessed by the probability integral transform (PIT), i.e. the predictive cumulative distribution function \widehat{F} evaluated at the observation t . If \widehat{F} is probabilistically calibrated, the PIT will be uniformly distributed, $\widehat{F}(t) \sim U([0, 1])$. To summarize the marginal calibration across grid point locations, we investigate the first two moments of the marginal PIT distribution over all time points in the validation period. A uniform distribution $U([0, 1])$ has an expectation of 0.5 and a standard deviation of $1/(2\sqrt{3}) \simeq 0.29$. It follows that $\mathbb{E}(\widehat{F}(t)) < 0.5$ indicates a positive bias and $\mathbb{E}(\widehat{F}(t)) > 0.5$ indicates a negative bias. If $\text{SD}(\widehat{F}(t)) < 0.29$, the forecast is overdispersive, and reversely, for $\text{SD}(\widehat{F}(t)) > 0.29$, it is underdispersive.

We assess multivariate calibration as proposed by Thorarinsdottir et al. (2016). Here, pre-rank functions are employed to map an ensemble of realizations from the multivariate forecast and the observation to real numbers which are subsequently ranked in a standard manner. If the forecast and the observations are statistically indistinguishable, the resulting histogram over the observation ranks is flat, whereas deviations from uniformity indicate miscalibration. (Thorarinsdottir et al., 2016) propose two pre-rank functions which assess the multivariate calibration in slightly different manners. The average pre-rank function

finds the average of the marginal univariate ranks while band depth ranking assesses the centrality of the observation within the forecast ensemble as proposed by López-Pintado and Romo (2009).

Forecast accuracy is typically assessed using proper scoring rules (Winkler and Murphy, 1968; Gneiting and Raftery, 2007). Scoring rules assign a numerical score to each forecast-observation pair, where a lower value indicates better predictive performance. To assess the marginal accuracy, we use the mean squared error (MSE),

$$\text{MSE}(\widehat{F}, t) = (\widehat{\mu} - t)^2,$$

where $\widehat{\mu}$ denotes the mean of \widehat{F} (Gneiting, 2011), and the continuous ranked probability score (CRPS),

$$\text{CRPS}(\widehat{F}, t) = \mathbb{E}_{\widehat{F}}|X - t| - \frac{1}{2}\mathbb{E}_{\widehat{F}}\mathbb{E}_{\widehat{F}}|X - X'|,$$

where \widehat{F} is a forecast distribution with a finite first moment and $X, X' \sim \widehat{F}$ denote two independent random variables. For an ensemble $\mathbf{x} = \{x_1, \dots, x_N\}$, the CRPS equals

$$\text{CRPS}(\mathbf{x}, t) = \frac{1}{N} \sum_{k=1}^N |x_k - t| - \frac{1}{2N^2} \sum_{k=1}^N \sum_{l=1}^N |x_k - x_l|.$$

The MSE is fast to compute and compares different mean models for the predictive distribution. The CRPS provides a more complete picture in that it assesses both calibration and sharpness (Gneiting and Raftery, 2007).

For a multivariate assessment we utilize the multivariate variogram score (VS) proposed by Scheuerer and Hamill (2015). For a multivariate distribution function \widehat{F} and an observation vector \mathbf{t} at S locations, the VS of order p is given by

$$\text{VS}(\widehat{F}, \mathbf{t}) = \sum_{i=1}^S \sum_{j=1}^S \omega_{ij} (|t_i - t_j|^p - \mathbb{E}_{\widehat{F}}|X_i - X_j|^p)^2,$$

where t_i is the observation at the i th location and X_i the i th component of a random vector distributed according to \widehat{F} . The (nonnegative) weights ω_{ij} are set to be constant, such that

the correlation structure of all distances is assessed, and we select the order $p = 0.5$, as recommended by Scheuerer and Hamill (2015).

To test significance of score differences, we apply a permutation test relying on resampling (Möller et al., 2013; Good, 2013). Two predictive distributions \widehat{F}_1 and \widehat{F}_2 are compared under a scoring rule $S(F, \cdot)$ using the statistic

$$s := \frac{1}{n} \sum_{i=1}^n (S(\widehat{F}_1, y_i) - S(\widehat{F}_2, y_j)) =: \frac{1}{n} \sum_{i=1}^n S_i. \quad (6)$$

The permutation test is then based on resampling copies of s with the labels of \widehat{F}_1 and \widehat{F}_2 swapped for a random number of summands. Under the null hypothesis, \widehat{F}_1 and \widehat{F}_2 perform equally well and the permutations would have the same limiting distribution as the statistic, s , as $n \rightarrow \infty$. By considering the rank of the observed statistic within the permutations, an asymptotic test is obtained. Permutation tests are computationally efficient and unlike the commonly applied Diebold-Mariano test (Diebold and Mariano, 1995), they do not require the estimation of the asymptotic variance of the score difference S_i which can be involved in the spatial dependence context.

Let us finally remark that validating forecasts in a high dimensional setting is a challenge in its own rights. For both variogram scores and multivariate rank histograms the role of the forecast dimension has been discussed in the original papers Scheuerer and Hamill (2015); Thorarinsdottir et al. (2016), and they were found to perform well in dimension S up to 20. When the dimension is much higher than that, and in particular larger than the number of available forecast-observation-couples, new issues arise. For example, the variogram score becomes computationally involved as the number of summands is S^2 . For multivariate rank histograms, on the other hand, slight misspecifications of the predictive marginal distributions tend to dominate the appearance of the histogram in very high dimension, making it less informative with regard to the multivariate predictive performance.

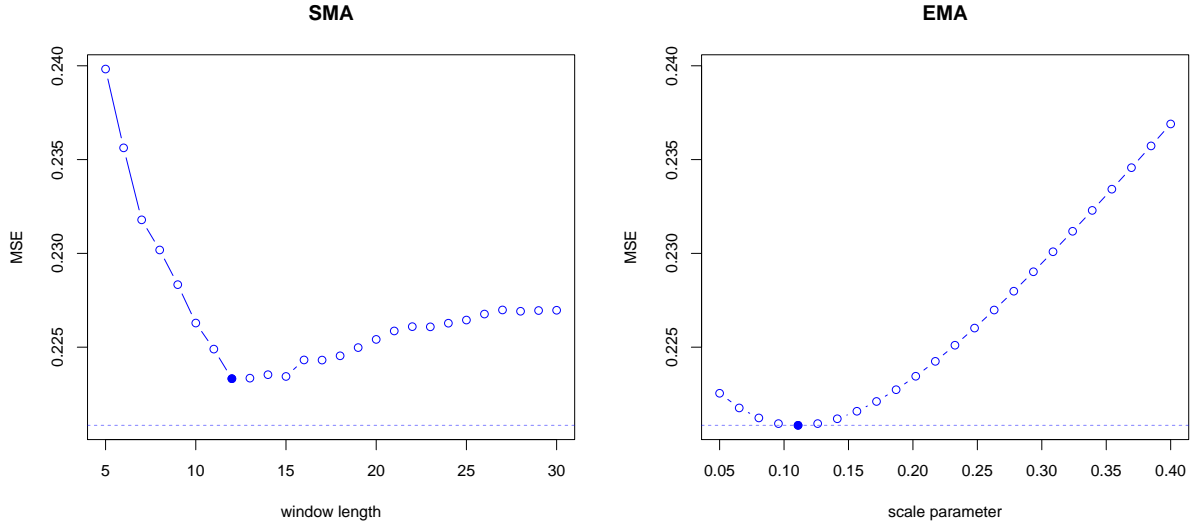


Figure 2: Mean squared error (MSE) of bias estimation by simple moving averages (SMA) for varying window length l (left), and for exponential moving averages (EMA) for varying scale parameter a (right), aggregated over all grid points, months and years 1995–2016. The horizontal dashed lines indicate the overall minimum MSE and the filled dots indicate the minimum MSE for each method. The overall minimum is reached for the EMA method with $a = 0.11$.

4 Results

4.1 Training period

The first step of the analysis is to determine optimal weighting parameters in Equation (2). For simple moving averages and window length l , the corresponding weights are $w_k = \mathbb{1}\{k \leq l\}/l$, while for exponential moving averages with scale parameter a the weights are $w_k \sim \exp(-ak)$, for the k th preceding year. For the bias-correction, the weighting parameters are chosen for each year in the validation period by minimizing MSE as follows:

For a range of weighting parameters, we bias-correct a set of previous forecasts in an out-of-sample fashion and compute the MSE. We then select the weighting parameter for which the MSE is minimized. Figure 2 shows this selection process for 2017. Here, the best performance is obtained for relatively short training periods of $l = 12$ for SMA and $a = 0.11$ for EMA, with a substantial improvement in the predictive performance under EMA. For the variance estimation, the weighting parameters are estimated by minimizing the CRPS. Here, the improvement by using weighted averages is more marginal and unweighted averages lead to close to optimal results. Furthermore, the optimal training period is usually somewhat longer than for the bias-correction. For 2017, the values would be $l = 28$ for SMA and $a = 0.05$ for EMA. The values are typical for years for which sufficient past training data is available.

4.2 Marginal predictive performance

For a more formal skill assessment, we compare the aggregated MSE for the SMA and EMA methods against the three NGR reference method. The results are summarized in Table 1. The NGR_m method performs substantially worse than all others, demonstrating that model biases strongly depend on location. Further, $NGR_{m,s}$ performs significantly better than NGR_s , indicating that the bias also varies between seasons. Both SMA and EMA outperform $NGR_{m,s}$, with EMA yielding the overall lowest value as demonstrated in Figure 2. The $NGR_{m,s}$ model relies on a total of approximately 10^6 parameters while the SMA and EMA approaches rely on one parameter each and are thus much more robust towards outliers. The significance of score differences is assessed by permutation tests, and the score of a method is printed in bold if it achieved the best result, or the score difference to the best model is not significant at a level of 5%. We apply this convention throughout the rest of the paper.

We continue our analysis using EMA for the bias-correction. Different models for es-

Method	NGR_m	NGR_s	$NGR_{m,s}$	SMA	EMA
MSE	2.028	0.417	0.227	0.223	0.220

Table 1: Mean squared error (MSE) over all grid points, months and years in the validation period 2001-2016. NGR_m is linear regression grouped by month, NGR_s by location, and $NGR_{m,s}$ by both, SMA is bias correction by simple moving averages, EMA by exponential moving averages. The best method is indicated in bold.

Method	NGR_m	NGR_s	$NGR_{m,s}$	SMA	EMA
CRPS	0.242	0.235	0.231	0.229	0.229

Table 2: Continuous ranked probability score (CRPS) for different variance estimation methods with bias-correction by EMA. Results are aggregated over all grid points, months and years in the validation period 2001-2016 and the best models are indicated in bold.

estimating marginal variances are compared in Table 2 using the CRPS. While the scores are similar for all methods, permutation tests reveal the score differences between moving averages and reference methods to be significant at a 5 % significance level. However, there is not a significant difference between SMA and EMA.

The calibration of EMA and the best NGR method, $NGR_{m,s}$ are assessed in Figure 3. The postprocessed forecasts are overall well calibrated, indicated by a white color. However, the PIT values reveal small biases in the region governed by the Gulf stream and in the southern oceans below -50° south. The PIT mean values for the EMA method are between 0.26 and 0.72 for all locations, while they range from 0.23 to 0.78 for the $NGR_{m,s}$. The figure indicates that the $NGR_{m,s}$ method exhibits similar biases as the exponential moving average approach, but tends to have larger biases overall. Figure 4 further shows the PIT standard deviations across locations for EMA, indicating overall good calibration except in the polar regions where the forecast is somewhat overdispersed.

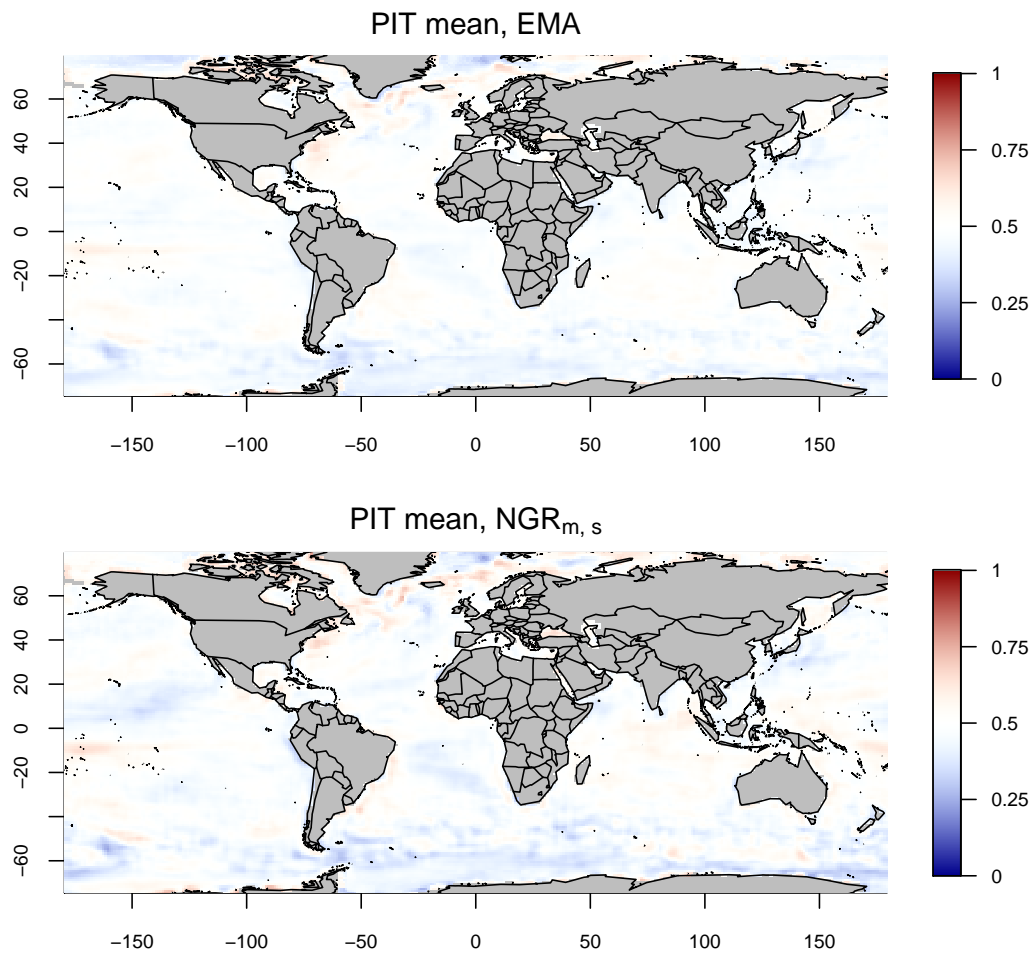


Figure 3: The probability integral transform (PIT) mean values in the validation period 2001–2016 at all locations for EMA (top) and $NGR_{m,s}$ (bottom). White color corresponds to the mean of a uniform random variable, indicating a calibrated forecast. Red shaded areas indicate a negative bias, while blue shaded areas indicate a positive bias.

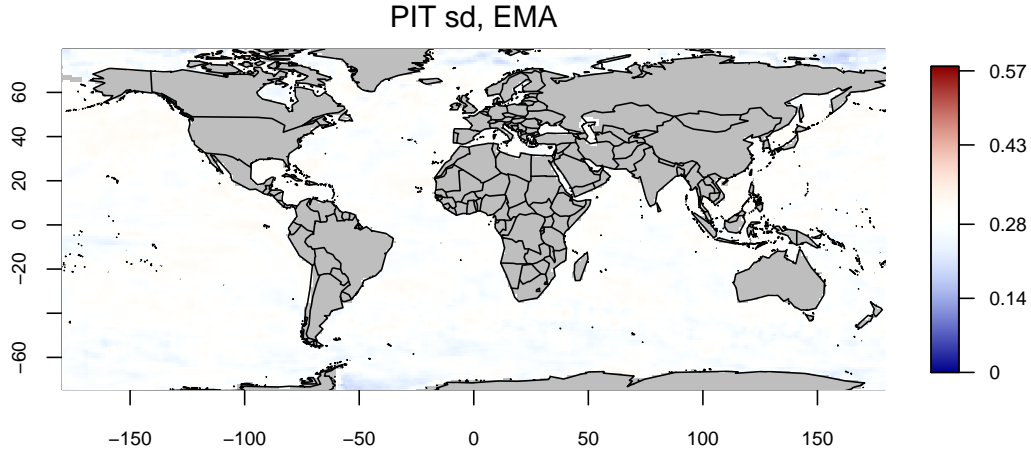


Figure 4: The probability integral transform (PIT) standard deviation in the validation period 2001–2016 at all locations for EMA. White color corresponds to the standard deviation of a uniform random variable, indicating a calibrated forecast. The red shaded areas indicate underdispersion and the blue shaded areas indicate overdispersion.

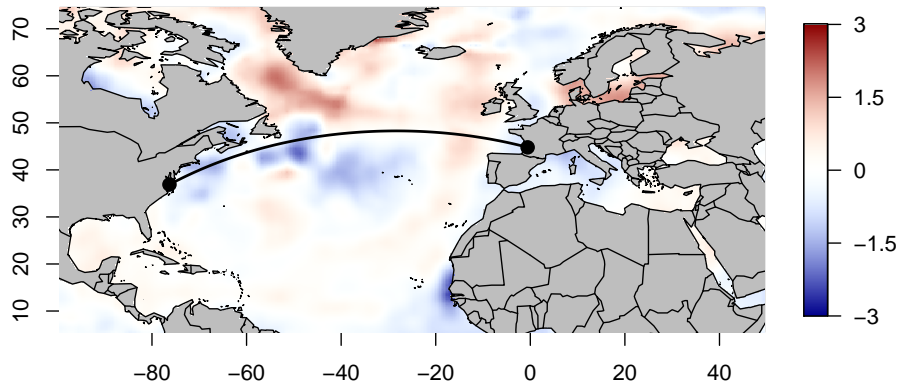


Figure 5: Observed forecast residuals in the North-Atlantic for June 2016 with the forecast issued at a lead time of 3 months. The geodesic connecting Norfolk, USA and Bordeaux, France that is considered as shipping route in our case study is shown in black.

Method	$\widehat{\Sigma}^{mc}$	$\widehat{\Sigma}^{ac}$	GS	ECC
VS(F, \mathbf{y})	0.03074	0.03075	0.03410	0.03111

Table 3: Variogram scores for the area shown in Figure 5 averaged over all months in the validation period 2001–2016. The best methods are indicated in bold.

4.3 Multivariate predictive performance

Here, we compare various multivariate postprocessing approaches where the marginal distributions are generated with EMA. For computational reasons, we restrict our analysis to an area covering the northern half of the Atlantic ocean, cf. Figure 5. The restricted area covers approximately 5600 grid points. Figure 5 shows the forecast residual, the difference between mean forecast and observations, for June 2016. The aim is for the multivariate correlation structure of the predictive distribution to produce similar spatial patterns. To assess this, we compare the methods in terms of variogram scores. To compute the variogram score, the moments of the predictive distribution, $\mathbb{E}_F[|X_i - X_j|^{1/2}]$ are estimated using 500 simulations from the distribution. For the ECC, the 9 forecast ensemble members are used instead. Table 3 shows the variogram scores averaged over all months in the validation period, with the significance of the score differences assessed by the permutation test. The lowest variogram score is achieved by the regularized covariance matrix with multiplicative correction, $\widehat{\Sigma}^{mc}$, and the score is significantly lower than those for both the geostationary and ECC approach, at a 5% level. The regularized covariance approach with additive correction, $\widehat{\Sigma}^{ac}$, achieves a similar variogram score as $\widehat{\Sigma}^{mc}$, with a non-significant score difference at the 5% level.

An empirical assessment of simulated residulas (not shown) suggests that the regularization approach produces the most realistic spatial structure. The residuals generated by the geostationary approach look somewhat too coarse. This is likely caused by an overall poor fit of the parametric variogram to the empirical variogram, resulting in an overesti-

Method	$\hat{\Sigma}^{mc}$	$\hat{\Sigma}^{ac}$	GS	ECC
MSE	0.686	0.698	0.723	0.709
CRPS	0.441	0.443	0.453	0.462

Table 4: Scores for minimum SST forecasts along a shipping route from Bordeaux, France to Norfolk, USA for the four different multivariate models, aggregated over all months and years in the validation period 2001–2016.

mation of the nugget. The residuals generated by ECC, on the other hand, seem to vary too little on a large scale, which is mainly caused by the low number of only 9 ensemble members.

5 Case study

In a further assessment of the multivariate predictive distributions, we take a more applied angle and use the model to predict the minimum SST along a shipping route crossing the Atlantic Ocean from Bordeaux, France to Norfolk, USA, see Figure 5. The route has a length of 6205 km and we consider all grid cells that are intersected by the geodesic from Bordeaux to Norfolk a part of the route, a total of 93 grid cells. The minimum SST along this route depends jointly on the SST at all locations along the route, requiring spatially coherent forecasts. We consider the same methods of multivariate postprocessing as in the previous section, i.e. the regularization approach, both with multiplicative and additive correction of the marginal variance, as well as the geostationary model and ECC as reference.

For each method, we generate multiple simulations from the predictive distribution for each month of the validation period, and compute the minimum temperature along the route. The empirical distribution of simulated minima is then considered the proba-

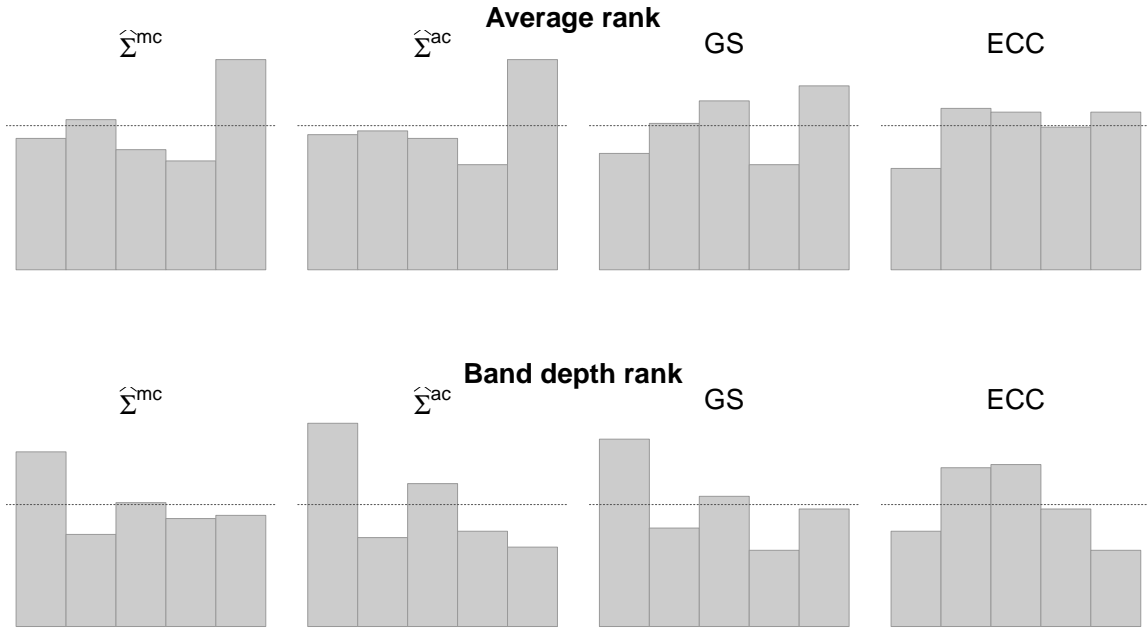


Figure 6: Average and band depth rank histograms for the four multivariate methods aggregated over all 192 months in the validation period 2001–2106. The dotted horizontal lines correspond to a perfectly uniform rank histogram.

bilistic forecast of the minimum temperature along the route. For the regularization and geostationary approaches, we simulate 500 forecasts each, whereas for ECC the postprocessed ensemble containing 9 members is used. The accuracy of the forecasts is evaluated with the univariate scores MSE and CRPS, see Table 4. Permutation tests show that the score differences between the regularization approaches with multiplicative and additive correction of the marginal distribution is not significant at a level of 5%, whereas both the geostationary model and ECC show lower skill.

We further assess the multivariate calibration of the 93-dimensional forecasts using average and band depth ranking, see Figure 6. Note that the number of available observations in the test set is only 192, making it necessary to restrict the number of bins. The rank his-

tograms of the regularization techniques and the geostationary approach look very similar. In fact, the correlation of the observation ranks is approximately 0.99 for any two of these methods, indicating that deviations from uniformity are mainly attributed to imperfect marginal calibration. All three methods exhibit too many high average ranks, corresponding to an overall underestimation of the temperature along the route, possibly caused by warming trends not accounted for in the numerical model. The same effect is responsible for too many low band depth ranks, signaling non-centrality of the observation within the ensemble.

The band depth rank histograms for ECC, however, display a slight \cap -shape indicating too strong spatial correlations in the empirical copula of the raw NWP ensemble. This is supported by plots of members from the raw ensemble forecast which tend to be visibly smoother than the observation (not shown). The average rank histogram for ECC looks more uniform than those for the other methods. This is presumably caused by the use of equally spaced quantiles which leads to a more evenly spread out predictive ensemble than any ensemble based on simulation. However, this comes at the cost of a very limited ensemble size.

6 Discussion

This paper proposes a fully probabilistic post-processing approach for multivariate forecasts, the computational costs of which scale well to higher dimensions. The proposed method incorporates a moving average approach combined with regularization of the covariance matrix through tapering. The approach yields a predictive distribution allowing for non-stationary, non-isotropic and negative correlations in the forecasting error. Based on validation data, it performs well with little available training data and is therefore attractive for seasonal and long-range weather predictions.

We have applied the method to seasonal forecasts of sea surface temperature issued

by the Norwegian Climate Prediction Model. Performance comparisons indicate that our methodology has higher predicting skill than current reference methods, specifically empirical copula coupling and a geostationary method. The geostationary method assumes the forecast error to have a positive and stationarity correlation structure, which in weather forecasting is a highly restrictive assumption, as the underlying physics in numerical prediction models will depend on geographic features not taken into account.

For the covariance tapering we chose the range of our tapering function to be 2500 km. At the equator this corresponds to 22 grid points in each direction. In our experiments, choosing any range between 1000 and 4000 km led to good results and did not affect the conclusions derived from Sections 4 and 5. Given the very limited amount of data we refrained from attempting to fit the range parameter. We have investigated an additive and a multiplicative correction of the marginal variances of the multivariate model. While the results indicate no significant difference between the skill of these corrections, the multiplicative correction seemed to perform slightly better overall. As the additive correction does not recreate the marginal model (1) exactly, and is heavier computationally, the approach based on multiplicative correction should be preferred.

As emphasized by Van Schaeybroeck and Vannitsem (2018), a main challenge for post-processing of seasonal weather forecasts is the shortage of available training data. This is supported by the findings in Sections 4.2 and 4.3, which demonstrate the risk of overfitting when forecast distributions are estimated separately at each location. We utilized moving averages to estimate the biases and variances. Our approach estimates location-specific biases and variances, but we only need to determine a single, global, weighting parameter. Thus the approach will be more robust against outliers and computationally faster than non-homogeneous Gaussian regression grouped by month and location, the best performing reference model. Moreover, our moving average approach will account (to a certain extent) for the trends caused by global warming and the increase in reliability of temperature measurements over the last 30 years.

Future research directions include to consider ensemble information beyond the ensemble mean, for instance the single ensemble members. The good performance of ensemble copula coupling, considering the high number of locations and low number of ensemble members, indicates that the ensemble members do contain valuable information. Ensemble copula coupling relies fully on the empirical copula of the ensemble to capture the multivariate forecast structure, while our approach only considers variability around the ensemble mean. Combining both sources of information may be a fruitful way to extend post-processing techniques in the high-dimensional setting. Moreover, we have currently not considered interactions between different months or seasons throughout the year. Early exploratory analyses showed that including information from previous months as predictors did not improved the forecast distribution. It seems, however, reasonable that forecast errors of different months may in fact be correlated and developing detailed models for such interactions may improve the predictive skill. Finally, our model does not account for sea ice in an appropriate way and could be improved by being combined with an external sea ice model.

References

- Boer, G. (2009). Climate trends in a seasonal forecasting system. *Atmos. ocean*, 47(2):123–138.
- Chilès, J.-P. and Delfiner, P. (1999). *Geostatistics: modeling spatial uncertainty*. John Wiley & Sons Inc., New York.
- Counillon, F., Bethke, I., Keenlyside, N., Bentsen, M., Bertino, L., and Zheng, F. (2014). Seasonal-to-decadal predictions with the ensemble Kalman filter and the Norwegian Earth System Model: a twin experiment. *Tellus A*, 66(1):21074.
- Counillon, F., Keenlyside, N., Bethke, I., Wang, Y., Billeau, S., Shen, M. L., and Bentsen,

- M. (2016). Flow-dependent assimilation of sea surface temperature in isopycnal coordinates with the Norwegian Climate Prediction Model. *Tellus A*, 68(1):32437.
- Dawid, A. P. (1984). Statistical theory: The prequential approach. *J. Roy. Statist. Soc. Ser. A*, 147:278–292.
- Diebold, F. X. and Mariano, R. S. (1995). Comparing predictive accuracy. *J. Bus. Econom. Statist.*, 13(3):253–263.
- Dobrynin, M., Domeisen, D., Müller, W., Bell, L., Brune, S., Bunzel, F., Düsterhus, A., Fröhlich, K., Pohlmann, H., and Baehr, J. (2018). Improved teleconnection-based dynamical seasonal predictions of boreal winter. *Geophys. res. lett.*, 45(8):3605–3614.
- Feldmann, K., Scheuerer, M., and Thorarinsdottir, T. L. (2015). Spatial postprocessing of ensemble forecasts for temperature using nonhomogeneous Gaussian regression. *Mon. weather rev.*, 143(3):955–971.
- Gaspari, G. and Cohn, S. (1999). Construction of correlation functions in two and three dimensions. *Q. j. roy. meteor. soc.*, 125(554):723–757.
- Gneiting, T. (2002). Compactly supported correlation functions. *J. Multivariate Anal.*, 83(2):493–508.
- Gneiting, T. (2011). Making and evaluating point forecasts. *J. Amer. Statist. Assoc.*, 106:746–762.
- Gneiting, T., Balabdaoui, F., and Raftery, A. E. (2007). Probabilistic forecasts, calibration and sharpness. *J. R. Stat. Soc. Ser. B. Stat. Methodol.*, 69:243–268.
- Gneiting, T., Raftery, A., Westveld, A., and Goldman, T. (2005). Calibrated probabilistic forecasting using ensemble model output statistics and minimum CRPS estimation. *Mon. weather rev.*, 133(5):1098–1118.

- Gneiting, T. and Raftery, A. E. (2007). Strictly proper scoring rules, prediction, and estimation. *J. Amer. Statist. Assoc.*, 102:359–378.
- Good, P. (2013). *Permutation tests: a practical guide to resampling methods for testing hypotheses*. Springer Science & Business Media.
- Ho, C. K., Hawkins, E., Shaffrey, L., Bröcker, J., Hermanson, L., Murphy, J. M., Smith, D. M., and Eade, R. (2013). Examining reliability of seasonal to decadal sea surface temperature forecasts: The role of ensemble dispersion. *Geophys. res. lett.*, 40(21):5770–5775.
- Hoskins, B. (2013). The potential for skill across the range of the seamless weather-climate prediction problem: a stimulus for our science. *Q. j. roy. meteor. soc.*, 139(672):573–584.
- Kolstad, E. W. and Årthun, M. (2018). Seasonal prediction from arctic sea surface temperatures: Opportunities and pitfalls. *J. climate*, 31(20):8197–8210.
- López-Pintado, S. and Romo, J. (2009). On the concept of depth for functional data. *J. Amer. Statist. Assoc.*, 104(486):718–734.
- McTaggart-Cowan, R., Davies, E., Fairman Jr., J., Galarneau Jr., T., and Schultz, D. (2015). Revisiting the 26.5°C sea surface temperature threshold for tropical cyclone development. *B. am. meteorol. soc.*, 96(11):1929–1943.
- Messner, J., Mayr, G., and Zeileis, A. (2017). Nonhomogeneous boosting for predictor selection in ensemble postprocessing. *Mon. weather rev.*, 145(1):137–147.
- Möller, A., Lenkoski, A., and Thorarinsdottir, T. (2013). Multivariate probabilistic forecasting using ensemble Bayesian model averaging and copulas. *Q. j. roy. meteor. soc.*, 139(673):982–991.

- Reynolds, R., Smith, T., Liu, C., Chelton, D., Casey, K., and Schlax, M. (2007). Daily high-resolution-blended analyses for sea surface temperature. *J. climate*, 20(22):5473–5496.
- Schefzik, R. (2016). A similarity-based implementation of the Schaake shuffle. *Mon. weather rev.*, 144(5):1909–1921.
- Schefzik, R. and Möller, A. (2018). Ensemble postprocessing methods incorporating dependence structures. In *Statistical Postprocessing of Ensemble Forecasts*, pages 91–125. Elsevier.
- Schefzik, R., Thorarinsdottir, T. L., and Gneiting, T. (2013). Uncertainty quantification in complex simulation models using ensemble copula coupling. *Stat. sci.*, 28(4):616–640.
- Scheuerer, M. and Hamill, T. M. (2015). Variogram-based proper scoring rules for probabilistic forecasts of multivariate quantities. *Mon. weather rev.*, 143(4):1321–1334.
- Thorarinsdottir, T. L., Scheuerer, M., and Heinz, C. (2016). Assessing the calibration of high-dimensional ensemble forecasts using rank histograms. *J. comput. graph. stat.*, 25(1):105–122.
- Van Schaeybroeck, B. and Vannitsem, S. (2018). Postprocessing of long-range forecasts. In *Statistical Postprocessing of Ensemble Forecasts*, pages 267–290. Elsevier.
- Vannitsem, S., Wilks, D., and Messner, J. (2018). *Statistical postprocessing of ensemble forecasts*. Elsevier Academic Press, 1st edition.
- Wilks, D. (2018). Univariate ensemble postprocessing. In *Statistical Postprocessing of Ensemble Forecasts*, pages 49–89. Elsevier.
- Winkler, R. L. and Murphy, A. H. (1968). “Good” probability assessors. *J. appl. meteorol.*, 7:751–758.